Report of the National Research Institute for Earth Science and Disaster Prevention, No. 59 ; March, 1999

Evaporation from Non-homogeneous Ground Surfaces : A Wind Tunnel Investigation

By

Tokuo KISHII*, Fumi SUGITA**

**National Research Institute for Earth Science and Disaster Prevention, Tsukuba, Ibaraki, 305-0006 Japan*

***Chiba University of Commerce, Ichikawa, Chiba, 272-8512 Japan*

Abstract

The flux-profile relationships over non-homogeneous ground surfaces were investigated in detail using a wind tunnel facilitated with a weighing lysimeter at NIED. The flow over a non-homogeneous rough surface become homogeneous above a certain height enabling the flux-profile relationships for homogeneous surface to be adopted for non-homogeneous surfaces using "effective" parameters. The "effective" parameters, however, suggest that the surface non-homogeneity which is a perturbation part of the obstacle distribution has a significant effect on roughness properties and that non-homogeneous surfaces exhibit the roughness properties of a homogeneous surface with a greater degree of average roughness. It was also found that the momentum roughness lengths of the non-homogeneous surfaces are significantly greater than scalar roughness lengths. These results may contribute to the estimation of input parameters for large scale evaporation models which simulate evaporation from heterogeneous surfaces.

Key words: Evaporation, Non-homogeneous surface, Wind tunnel, Flux-profile relationships

1. Introduction

Evaporation of water in the natural environment is one of the important processes in the hydrological cycle of the earth. The hydrological cycle is a closed cycle of water transfer through the atmosphere, the earth surface, and the subsurface. Water is removed from the ground surface by evaporation and becomes unavailable to human beings as a water resource. Evaporation which is the vaporization of water also involves energy transfer, so that it has a significant effect on other surface fluxes such as momentum transfer and heat transfer between the ground surface and the atmosphere. The relationships between the surface fluxes of momentum, heat and vapour, and the mean profiles of wind velocity, potential temperature and specific humidity over homogeneous surfaces are well described by the three flux-profile equations based on the Monin-Obukhov similarity theory shown below (Brutsaert, 1982). The "mean" in this study refers to the average over a certain time period.

$$\bar{u}=\frac{u_*}{k}\left[\ln\left(\frac{z-d_0}{z_{0m}}\right)-\Psi_m(\zeta)\right] \tag{1}$$

$$\bar{\theta}=\theta_s-\frac{H}{ku_*\rho C_p}\left[\ln\left(\frac{z-d_0}{z_{0h}}\right)-\Psi_h(\zeta)\right] \tag{2}$$

$$\bar{q}=q_s-\frac{E}{ku_*\rho}\left[\ln\left(\frac{z-d_0}{z_{0v}}\right)-\Psi_v(\zeta)\right] \tag{3}$$

where

$$\zeta=\frac{z}{L} \tag{4}$$

$$L=\frac{\rho C_p\theta u_*^3}{kgH} \tag{5}$$

$\bar{u}$ is the mean wind velocity, u_* the friction velocity, k the von Kàrmàn constant, z the height above the sand surface, d_o the zero-plane displacement height, z_{om}, z_{oh}, z_{ov}, the roughness lengths for momentum, heat and vapour, respectively, ψ_m, ψ_h, ψ_v, the stability

correction functions for momentum, heat and vapour, respectively, $\bar{\theta}$, the mean potential temperature,

θ_s, the surface potential temperature, H the sensible heat flux, ρ, the air density, C_p the specific heat, $\bar{q}$, the mean specific humidity, q_s the surface specific humidity, E the water vapour flux, and g, the gravitational acceleration.

Since most actual surfaces are non-homogeneous, these flux-profile equations for homogeneous surfaces are often applied to heterogeneous surfaces. The surface non-homogeneity is lumped into "effective" parameters in such cases. This is based on the idea that a non-homogeneous surface can be represented by an equivalent homogeneous surface with some "effective" parameters. Thus, for instance, momentum transfer from a non-homogeneous surface is described by the momentum transfer equation for a homogeneous surface (Equation (1)) with an "effective" z_{om} and an "effective" u_* values which account for the effect of the physical non-homogeneity of the surface on the momentum transfer.

Many laboratory (Buckles *et al.*, 1984), numerical (*e.g.* Wood and Mason, 1993) and field (*e.g.* Kustas and Brutsaert, 1986, Grant and Mason, 1990) studies support the validity of this approach for momentum fluxes when the scale of the surface non-homogeneity is small compared to the depth of the boundary layer and when the mean profile over the non-homogeneous surface is still logarithmic. Most of these studies reported that the "effective" z_{om}s were much larger than the local z_{om} values, suggesting that the use of local z_{om} values for large scale weather prediction / climate models may lead erroneous results.

Though some recent numerical studies (*e.g.* Wood and Mason, 1991) have also demonstrated good applicability of the "effective" parameter approach to describe heat and vapour transfer from non-homogeneous surfaces, the validity of this approach for these scaler fluxes in actual field needs to be further investigated.

The primary purpose of this study is to investigate the applicability of this "effective" parameter approach for heat and vapour transfers as well as for momentum transfer by means of laboratory wind tunnel experiments over physical roughness models. In particular, the properties of the three "effective" roughness lengths of non-homogeneous surfaces were examined in detail, and were compared to those of roughness lengths for homogeneous surfaces. Although the scale of the laboratory experiments is much smaller than the actual boundary layer, a close examination of the relationships between the mean profile and the surface fluxes over non-homogeneous surfaces in the laboratory should give some insight into the properties of the "effective" parameters of actual non-homogeneous surfaces in the field.

2. Experimental Arrangement

A series of wind tunnel experiments were conducted over surfaces with small scale heterogeneity in a closed circuit wind tunnel at the National Research Institute for Earth Science and Disaster Prevention. The schematic of the wind tunnel is shown in Fig. 1. The wind tunnel has an observation section of 1m by 1m in the cross section and is 3m in length, and is fitted with an underlying weighing lysimeter (1m in width, 3m in length and 0.6m in depth) packed with uniform fine sand.

A hot-cross wire anemometer(Model 1241-20, TSI Inc.), a hygrometer (Model HMP35A, Vaisala) and a thermocouple (Model SCPSS-040E-6, OMEGA) are installed on the movable sensor arm in the wind tunnel for two-dimensional or three dimensional profile measurements. The water table in the sand was maintained at a constant level (either 0.1 or 0.5m below the surface) to give a steady state water supply to the evaporating surface. Sixteen tentiometers, eighteen thermometers and two heat flux plates are also installed in the sand box. A removable radio meter (THRDS7, Radiation and Energy Balance System Inc.) was occasionally inserted into the wind tunnel to estimate the net radiation flux to the surface. The average soil surface temperature was measured by an infrared thermometer (Model 350, Everest Interscience Inc.) which was attached to the ceiling of the wind tunnel.

All experiments were conducted under steady state atmospheric as well as subsurface conditions. In -coming air was controlled to have a mean velocity of 1m/s, a temperature of 20/25 °C and a relative humidity of 60%. These gave almost neutral but slightly stable atmospheric conditions.

The first experiment was conducted over a smooth sand surface. Then the sand surface was covered with roughness obstacles which were cylinders or sand ridges as shown in Fig. 2a. One of these two types of obstacles were distributed either homogeneously or non-homogeneously on the surface for rough cases (*e.g.* Fig. 2b). The shortest separation distance between the cylinders was 5 cm in our experiments. The cylinders were distributed non-homogeneously or homogeneously to the mean wind direction and always homogeneously to the lateral direction (vertical to the mean wind direction). In order to restrict

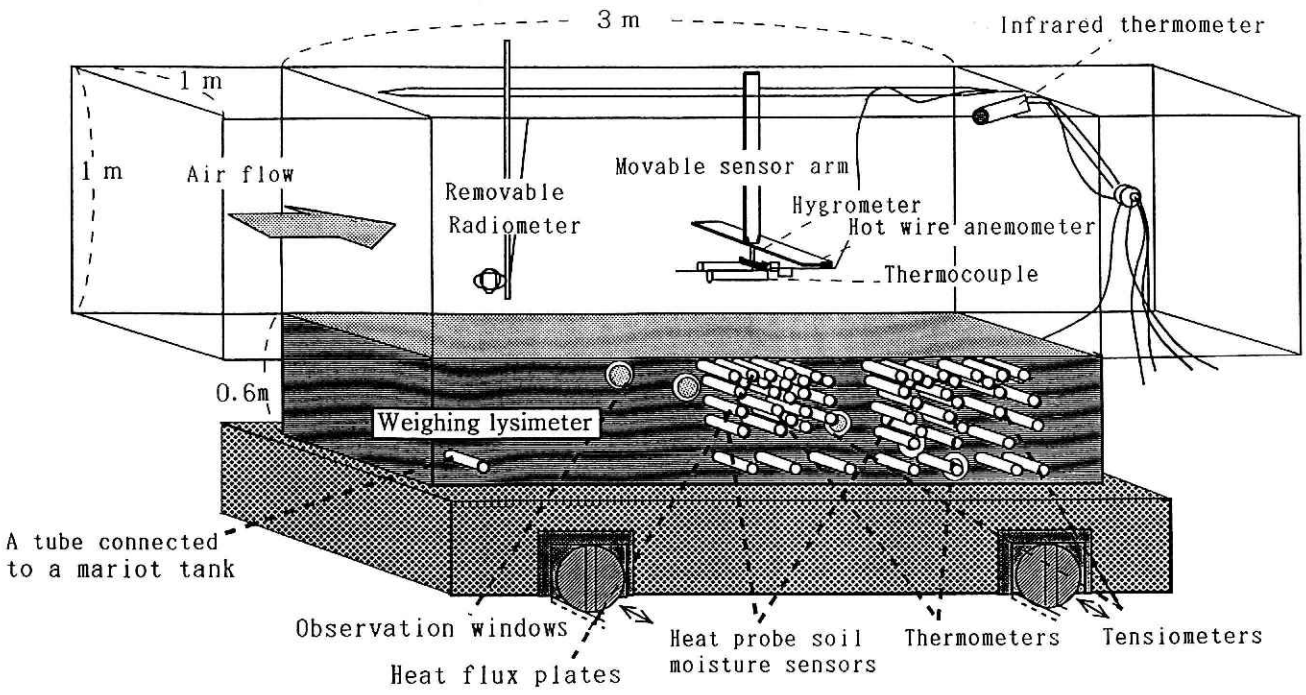

Fig. 1 Schematic of the wind tunnel.

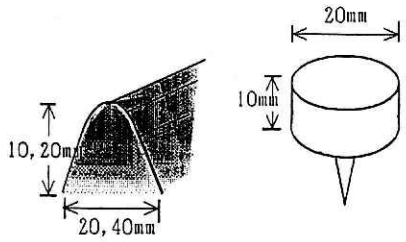

Fig. 2a Roughness obstacles: a single ridge obstacle and a single column obstacle.

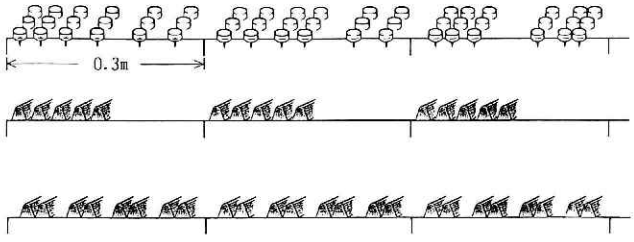

Fig. 2b Examples of the roughness obstacle distributions.

the heterogeneity to a small scale, every surface section of 0.3m in the main wind direction was set to have the same number of obstacles. Thus the roughness in these experiments is considered to be statistically homogeneous.

After the steady state of the subsurface and the atmospheric conditions were established, profiles of wind velocity, temperature and relative humidity were observed at 2.6m downwind in the wind tunnel. In total, experiments were conducted over 27 different surfaces.

3. Results and Discussions

3.1 Mean vertical profiles

Fig. 3 shows a typical $u'w'$ profile observed for rough surfaces. u' and w' are the turbulent fluctuation component of the mean wind velocity in main wind direction (u) and that in the vertical direction, respectively. Three distinct parts can be found in the

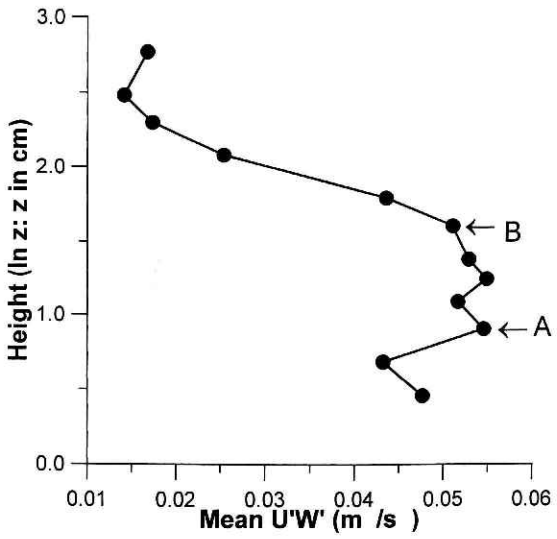

Fig. 3 An example of a typical $u'w'$ profile.

profile : an interfacial sublayer (below the height A in Fig. 3) where the turbulence is affected by each roughness element, a dynamic (constant flux) sublayer (between the heights A and B in Fig. 3) in which the effect of roughness elements is averaged over and $u'w'$ is almost constant with height, and an outer region (above the height B in Fig. 3) where the effect of the roughness is small and $u'w'$ decreases as the height increases. Although the scale is different, this structure of the profile found in the wind tunnel is similar to that of the actual atmospheric boundary layer of the earth.

The mean wind velocity was observed simultaneously with $u'w'$ measurements for all cases. The mean wind velocity profile obtained corresponding to $u'w'$ profile shown in Fig. 3 is indicated in Fig. 4. Although the interfacial sublayer can not be recognized clearly in the profile shown in Fig. 4, the dynamic sublayer (between the heights A and B in Fig. 4) where the profile is almost log-linear, and the outer region (between the heights B and C in Fig. 4) can be found easily. The profile above the height C in Fig. 4 is the layer often referred to as free atmosphere, where no surface effect is found.

The length of the dynamic sublayer found in the mean wind velocity profile is always somewhat longer than the one found in the $u'w'$ profile. This log-linear region in the lower part of the each mean wind velocity profile, was fitted to the flux-profile equation (Equation (1)), using a non-linear least-squares fitting program (FIT, coded by van Genuchten, 1971).

The log-linear parts of the profile were also found in the mean temperature and the specific humidity profiles observed. These parts were also fitted to the semi-logarithmic flux-profile equations (Equations (2) and (3)). The length of the profile used for curve fittings were different from profile to profile, depending on the length of the log-linear part of each profile.

Due to almost neutral but slightly stable atmospheric conditions in our experiments, the stability correction functions were assumed to be,

$$\Psi_m = -5(\zeta - \zeta_{0m}) \tag{6}$$

$$\Psi_h = -5(\zeta - \zeta_{0h}) \tag{7}$$

$$\Psi_v = -5(\zeta - \zeta_{0v}) \tag{8}$$

where ζ_{0m}, ζ_{0h} and ζ_{0v} are the surface values of ζ for momentum, heat and vapour, respectively, and were assumed to be zero in our analysis. The potential temperature was replaced by temperature due to very small pressure variation in the system used in this study. In the three flux-profile equations(Equations (1),(2) and (3)), u_*, d_0, z_{0m}, H, z_{0h}, q_s, E, z_{0v} were optimized through curve fittings. Sometimes more than one best fit parameter sets were found because of these multiple parameter fittings. In such cases, one set which had the most appropriate d_o value that should be less than a single obstacle height was chosen.

Some examples of the results of the mean wind velocity curve fittings are shown in Fig. 5. Fig. 6 and 7 show examples of the mean temperature and the specific humidity profile curve fittings, respectively. Fairly good fits were found for all mean wind velocity profiles. Good fits were also found for most temperature and specific humidity profiles.

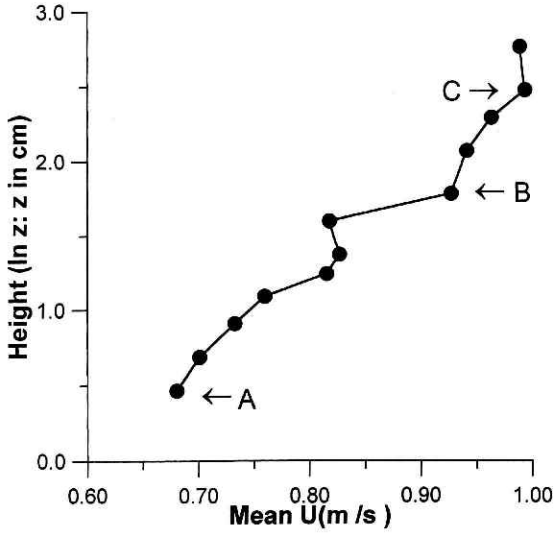

Fig. 4 The mean u of the profile shown in Fig. 3.

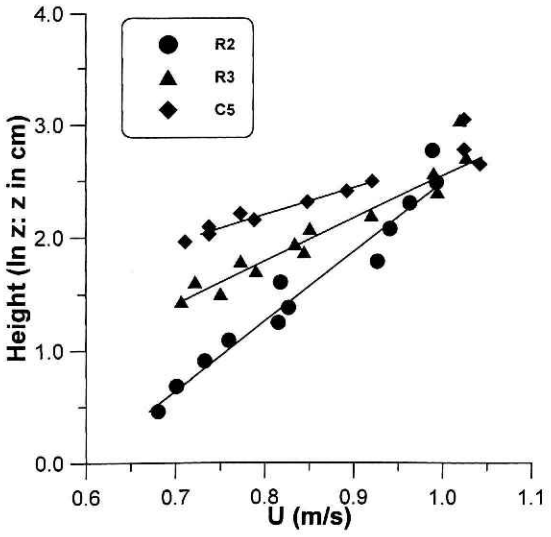

Fig. 5 Examples of the mean wind velocity profiles observed over non-homogeneous surfaces and fitted curves.

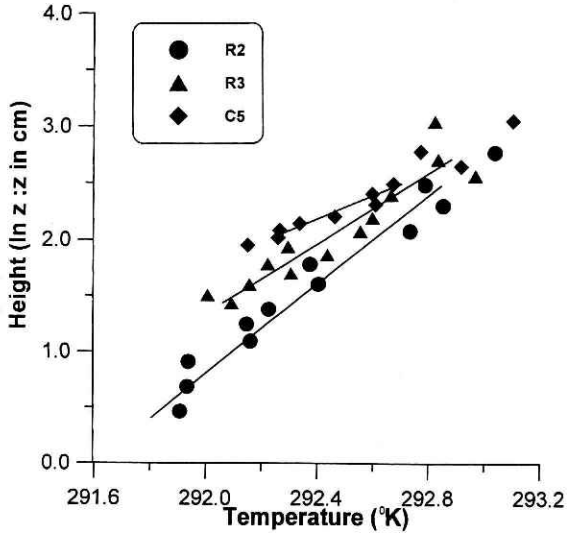

Fig. 6 Examples of the mean temperature profiles observed over non-homogeneous surfaces and fitted curves.

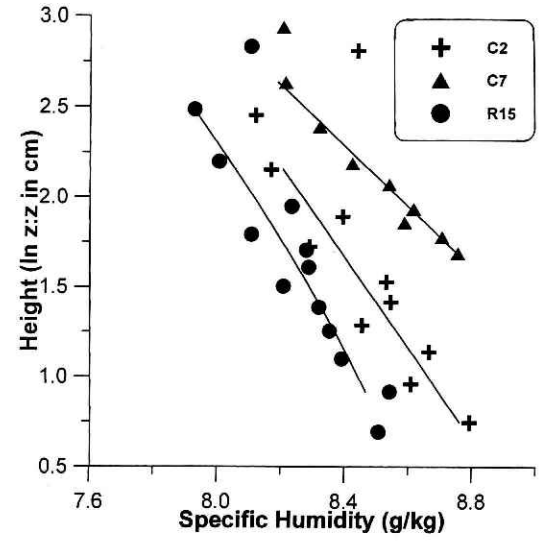

Fig. 7 Examples of the mean specific humidity profiles observed over non-homogeneous surfaces and fitted curves.

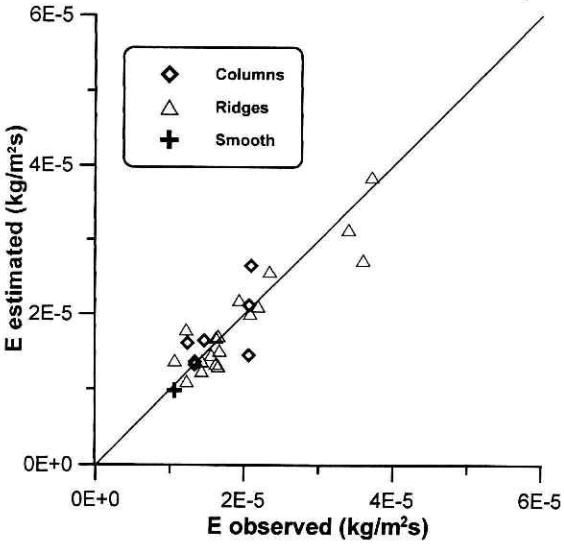

Fig. 8 The relationships between the evaporation rates estimeted by the mean profile methods and those observed by the weighing lysimeter.

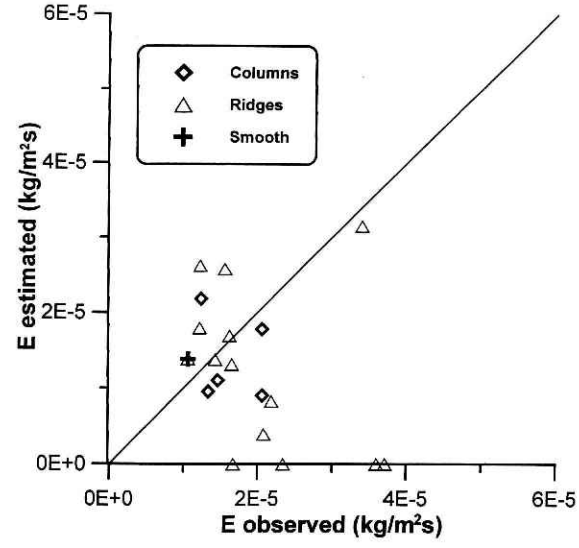

Fig. 9 The relationships between the evaporation rates estimated by the eddy correlation methods and those observed by the weighing lysimeter.

The evaporation rates (E) estimated by the curve fitting were plotted against the true values obtained by weighing (Fig. 8). An excellent agreement is found between the estimated and the true values for most homogeneous and non-homogeneous surfaces, suggesting a high reliability of the curves fitted.

The direct measurement of the evaporation rates in the atmosphere was also attempted by eddy correlation methods. In order to obtain the covariance of u' and q', the hot-cross wire anemometer and the Krypton hygrometer (KH20, Campbell Scientific Inc.) were placed in the constant flux layer (approximately 3cm above the ground surface). A single measurement was taken in 100Hz for 10 minutes. The calculated results are plotted against the true evaporation values in Fig. 9. Though the calculated E value of a smooth surface and those of almost half the rough surfaces agreed well with the true values, the rest show significant deviations from the true values. Most of them underestimate the fluxes, suggesting a poor correlation between u' and q' in these measurements. The separation distance of 2cm between the sensor of the anemometer and that of the hygrometer may be too large in this wind tunnel for these cases.

The sensible heat flux was estimated by calculating the energy budget at the ground surface for each surface setting. The energy budget at the ground surface is expressed as,

$$R_n = G - lE = H \tag{9}$$

where R_n, is the net radiative flux, G is the energy flux leaving the surface into the subsurface, l is the latent heat of vaporization. R_n was measured by the radio meter, and G was estimated by the observed values of the two heat flux plates buried at 3cm and 5cm below the sand surface. Substituting R_n, G and E obtained by weight measurements into Equation (9), H was calculated. The results are plotted against the estimated values by the profile curve fittings, and are shown in Fig. 10. A fairly good fit was found for most cases.

These agreements between optimized and observed or estimated fluxes of E and H suggest a high degree of accuracy of the other parameters(*e.g.* z_{0m}, z_{0h} and z_{0v}) optimized through the curve fittings.

3.2 Roughness lengths for momentum, heat and vapour

The roughness lengths estimated by profile fittings are summarized in Table 1. The z_{om} for the smooth sand surface is very small (in the order of 10^{-6} m), which is slightly smaller than most values reported for flat sand/mud surfaces. This is probably because the experiments were conducted on a very small scale, so that the surface physical properties were similar to those of smooth surfaces rather than flat sand surfaces in field scale. The z_{om}s for rough surfaces are two to four orders of magnitude larger than the z_{om}s for the smooth surface.

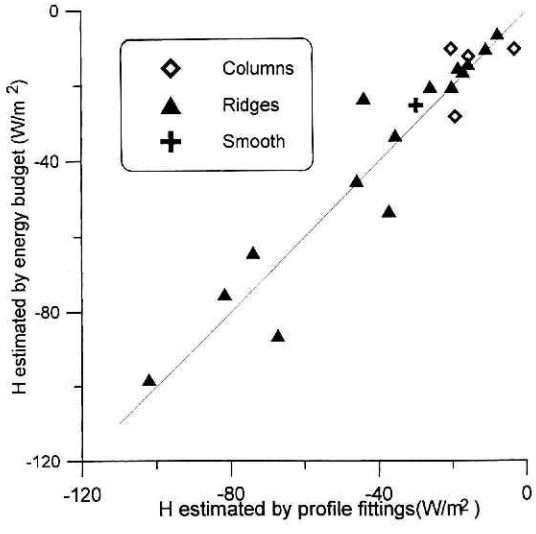

Fig. 10 The relationships between the sensible heat flux estimeted by the mean profile methods and those estimated by energy budget methods.

It was also found that the non-homogeneous rough surfaces have the "effective" z_{om}s of almost an order of magnitude greater than those for homogeneous rough surfaces for both obstacles. Since exactly the same number of obstacles are on every surface for the cylinder cases, the difference between the z_{om} values of homogeneous and those of non-homogeneous surfaces can be attributed to the differences in the distribution of obstacles. Specifically, the perturbation part of non-homogeneity is causing these differences since the average number of obstacles were homogeneously distributed in all experiments.

The ratio of z_{om}/z_{oh} and the ratio of z_{0m}/z_{0v} found for the smooth sand surface are not in unity which is often assumed in modeling studies. Small z_{om}/z_{ov} ratio may be due to the wet surface condition.

All z_{om}/z_{oh} and z_{om}/z_{ov} for rough surfaces are greater than unity. Thus, it is obvious that $z_{om}=z_{oh}=z_{ov}$ can not be assumed either for rough homogeneous or for non-homogeneous surfaces. Non-homogeneously rough surfaces with cylinders have an order of magnitude greater values of both z_{om}/z_{oh} and z_{om}/z_{ov} than those for homogeneously rough surfaces, while non-homogeneous surfaces with sand ridges have nine and six times greater ratios of z_{om}/z_{oh} and z_{om}/z_{ow}, respectively, compared to those for homogeneously rough surfaces.

Thus, it can be concluded that the surface non-homogeneity seems to serve as greater roughness and makes the momentum roughness length significantly greater than the scaler roughness length.

When $z_{om} \neq z_{oh}$, the surface temperature (θ_s) which is the temperature at $z=z_{0h}$ and the temperature at $z=z_{om}$ (θ_o) are not equal. Under neutral conditions, the difference between θ_s and θ_o can be expressed as,

$$\frac{\theta_0 - \theta_s}{\theta_*} = \frac{1}{k} ln\left(\frac{z_{0m}}{z_{0h}}\right) \tag{10}$$

where

Table 1 The arithmetical means of roughness properties.

	z_{0m}(m)	z_{0m}/z_{0h}	z_{0m}/z_{0v}
smooth	$6*10^{-6}$	2.3	0.2
cylinders			
homogeneous	$1.5*10^{-3}$	58.6	2.5
non-homogeneous	$2.2*10^{-2}$	1145.3	38.3
ridges			
homogeneous	$3.3*10^{-4}$	75.5	3.0
non-homogeneous	$3.3*10^{-3}$	681.5	18.3

$$\theta_* = -\frac{H}{\rho C_p u_*} \tag{11}$$

θ_s and θ_o was calculated based on the values of z_{om} and z_{oh}, and θ profile obtained by the curve fittings for each case. By substituting H and u_* obtained by the profile curve fittings into Equation(11), θ_* was also calculated and its relationship to $\theta_o - \theta_s$ is shown in Fig. 11. A linear curve was fitted to the data obtained from rough surfaces. The slope of the fitted curve was 15.551, which indicates the ratio of z_{om}/z_{om} would be 502.8 on average for these cases. The smooth surface cases do not agree with the fitted curve, indicating the ratio of z_{om}/z_{om} for the smooth surface is different from that for the rough surfaces.

In a similar way, the surface specific humidity(q_s) which is the specific humidity at $z = z_{ov}$ and q at $z = z_{0m}$ (q_o) is not equal, when $z_{ow} \neq z_{om}$. $q_o - q_s$ can be expressed as,

$$\frac{q_o - q_s}{q_*} = \frac{1}{\chi}\left(\ln\frac{z_{om}}{z_{ov}}\right) \tag{12}$$

where

$$q_* = \frac{lE}{\rho l u_*} \tag{13}$$

Fig. 12 shows the relationship between $q_o - q_s$ and q_* calculated based on the parameters obtained by the curve fittings. The slope of the fitted linear curve is 5.067, which indicates the ratio of z_{0m}/z_{0v} is 7.591 on average. Since many $q_o - q_s$ values of rough surfaces are zero, the reliability of the slope value for specific humidity is not very high. The $q_o - q_s$ for the smooth surface seem to agree with the fitted curve.

Though the geometrical average ratio values found by the above method are smaller than the ones obtained by arithmetical means (Table 1), z_{om}s are still shown to be significantly larger than the scaler roughnesses of z_{oh} or z_{ow} *for both homogeneous and non-homogeneous rough surfaces.*

It is known that z_{om}/z_{oh} and z_{oh}/z_{ov} are strong function of roughness Reynolds number (z_{o+}) (Brutsaert, 1975), which is defined as

$$z_{0+} = \frac{u_* z_0}{\nu} \tag{14}$$

where z_o is the roughness length($z_o = z_{om}$ was assumed in our analysis) and ν is the kinematic viscosity. The surfaces in our experiments were found to have the roughness Reynolds number of approximately 0.013 to 1500.

Fig. 13 shows the relationship between log (z_{om}/z_{ov}) and z_{o+} found in our experiments. Although the data for rough cases shows significant scattering, it generally obeys the curve predicted theoretically for homogeneous bluff-rough surfaces (Brutsaert, 1975)except extreamly rough cases.

Fig. 14 shows log (z_{om}/z_{oh}) and z_{o+} relationships. Although there is significant scattering again for rough surfaces, the data obtained for non-homogeneous surfaces also shows fairly good agreement with the theoretical curves predicted for homogeneous

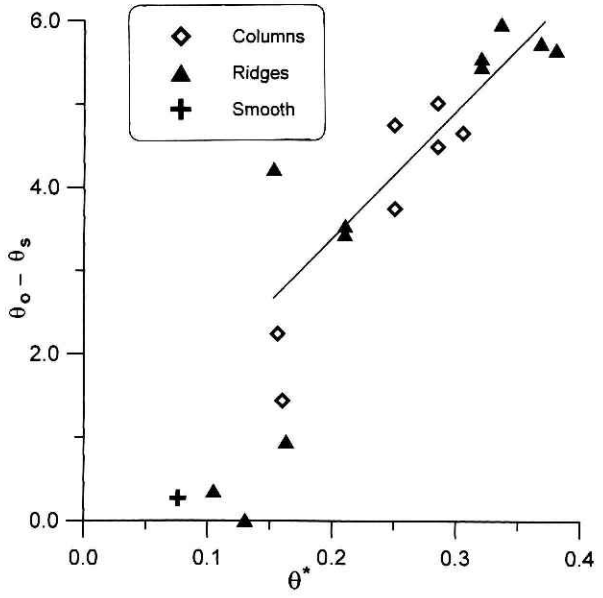

Fig. 11 The relationship between the near-surface temperature difference ($\theta_o - \theta_s$) and the temperature scale (θ^*).

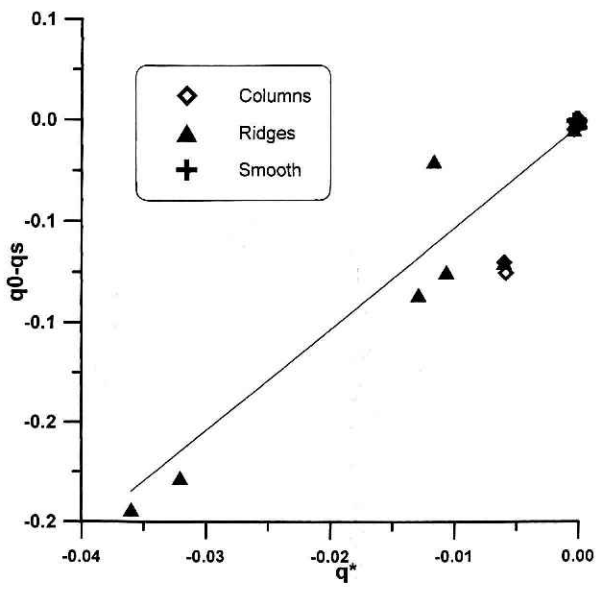

Fig. 12 The relationship between the near-surface specific humidity difference ($q_o - q_s$) *and the* specific humidity scale (q^*).

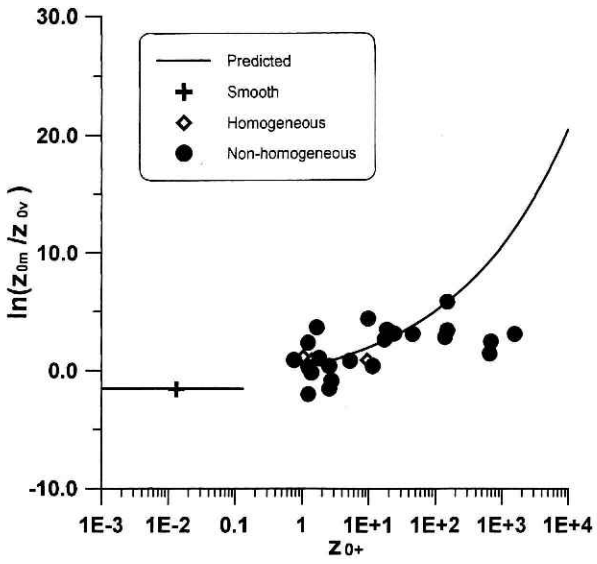

Fig. 13 The relationship between log (z_{om}/z_{ov}) and the roughness Reynolds number (z_{o+})

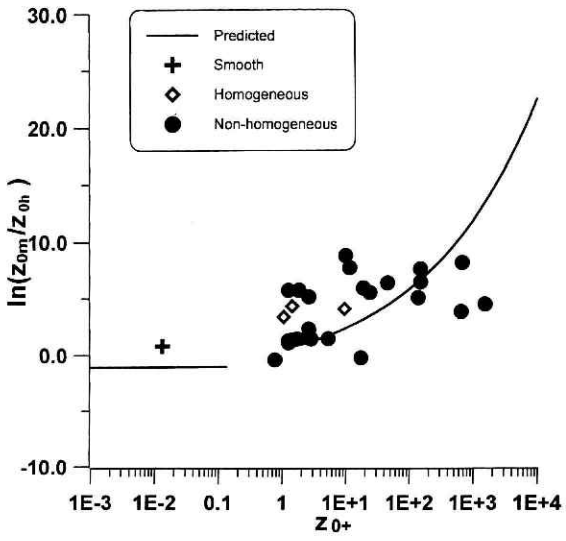

Fig. 14 The relationship between log (z_{om}/z_{oh}) and the roughness Reynolds number (z_{o+})

rough surfaces. The observed log (z_{om}/z_{ov}) scatters below the predicted curve, while log (z_{om}/z_{0h}) scatters somewhat above the predicted curve.

These results indicate that the properties of the "effective" roughness parameters for non-homogeneous surfaces are, in general, similar to those of roughness parameters for homogeneous surfaces. Thus, the relationship between the "effective" z_{om} and the "effective" scaler roughnesses (z_{oh} and z_{ov}) are also similar to those of homogeneous surfaces. The "effective" roughness parameter values found for the non-homogeneous surfaces, however, indicate that the average roughness of the equivalent homogeneous surfaces are significantly greater than the actual roughness of the non-homogeneous surfaces.

4. Conclusions

A series of wind tunnel experiments were conducted to study evaporation from non-homogeneous rough surfaces. The wind tunnel is fitted with weighing lysimeter uniformly packed with fine sand on which small columns or sand ridges are distributed as roughness obstacles. Under almost neutral, but slightly stable atmospheric and steady state subsurface conditions, the profiles of wind velocity, temperature and humidity were observed at 2.6m downwind in the wind tunnel for 27 different surfaces.

A semi-logarithmic region was found in the lower part of each profile, which was fitted to the flux-profile equations to estimate surface fluxes and the roughness parameters such as roughness lengths for momentum (z_{om}), heat (z_{oh}) and vapour (z_{ov}). The evaporation rates and the sensible heat fluxes estimated by the curve fittings agreed well with the true values obtained by weighing lysimeter and the estimated values obtained by heat budget method, respectively, indicating good reliability of other roughness parameters estimated by the curve fittings. The results are summarized as follows.

(1) The flow over non-homogeneous rough surfaces becomes homogeneous above a certain height, enabling "effective" parameters for the flux-profile equations to describe average surface fluxes can be found.

(2) The roughness properties of non-homogeneous surfaces are, in general, similar to those of homogeneous surfaces. A non-homogenous surface, however, exhibits the roughness properties of a homogeneous surface which has a greater degree of average roughness than the actual surface. Thus, it is concluded that non-homogeneity which is the perturbation part of obstacle distribution has a significant effect on roughness properties, and that perturbation in the obstacle distribution makes an equivalent homogeneous surface have a greater degree of average roughness than the actual non-homogeneous surface.

(3) The momentum roughness lengths of the non-homogeneous surfaces (*i.e.* "effective" z_{om}) are significantly greater than scaler roughness lengths(*i.e.* "effective" z_{oh} and z_{ov}) The difference between z_{om} and z_{oh} or z_{ov} of non-homogeneous surfaces are greater than that of homogeneous surfaces.

The actual surface physical properties which contribute and determine the values of these "effective"

surface parameters needs to be further investigated.

Acknowledgement

This study was supported by the STA project "Researches on mechanisms and impacts on climate change caused by global warming".

References

1) Blyth, E.M., Dolman, A.J. and Wood N. (1993): Effective resistance to sensible-and latent-heat flux in heterogeneous terrain, *Q.J.R. Meteorol. Soc.*, **119**, 423-442.

2) Brutsaert W.(1982): Evaporation into the atmosphere, D.Reidel Publishing Company, Dordrecht, Holland., 299p.

3) Brutsaert W.(1975): A theory for local evaporation (or heat transfer) from rough and smooth surfaces at ground level, *Water Resources Res.*, **11**, 543-550.

4) Buckles, J., Hanratty, T.J. and Adrian, R.J.(1984): Turbulent flow over large-amplitude wavy surfaces, *J. Fluid Mech.*, **140**, 27-44.

5) Grant A.L.M. and Mason, P.J.(1990): Observation of boundary-layer structure over complex terrain, *Q.J.R. Meteorol. Soc.*, **116**, 159-186.

6) Kustas, W. and Brutsaert, W.(1986): Wind profile constants in a neutral atmospheric boundary layer over complex terrain, *Boundary Layer Meteorology*, **34**, 35-54.

7) Wood, N. and Mason P.(1991): The influence of static stability on the effective toughness lengths for momentum and heat transfer, *Q.J.R. Meteorol. Soc.*, **117**, 1025-1056.

8) Wood, N. and Mason, P.(1993): The pressure force induced by neutral, turbulent flow over hills, *Q.J.R. Meteorol. Soc.*, **119**, 1233-1267.

(Accepted: September 2, 1998)

Report of the National Research Institute for Earth Science and Disaster Prevention, No. 59 ; March, 1999

不均質な地表面からの蒸発に関する風洞実験

岸井徳雄*・杉田　文**

防災科学技術研究所

要　旨

さまざまな不均質特性をもつ地表面からの蒸発に関する室内実験を，防災科学技術研究所・地表面乱流風洞実験施設を利用してこなった．不均質地表面上の気流はある一定高度より上では均質流となり，一般的に用いられている均質地表面に対するフラックス—プロファイル関係式を“有効”パラメータを導入することにより，そのまま不均質面に応用できることがわかった．ただし，不均質面から得られた“有効”パラメータの値は不均質性の特性が地表面の粗度特性に大きな影響を及ぼしていることを示し，一般に，不均質面は，実際よりも大きな平均粗度をもつ地表面の粗度特性を示す．また，不均質面におけるモーメントの粗度長は，一般に，顕熱や水蒸気の粗度長に比べはるかに大きな値であることが明らかとなった．これらの成果は“蒸発モデル”のパラメータ推定に有用な情報を与えるものである．

キーワード：蒸発，不均質地表面，風洞，フラックス—プロファイル関係式

*防災科学技術研究所

**千葉商科大学（防災科学技術研究所　客員研究官）